Extrapolating $(e, e'p)$ to (e, e')

Lawrence B. Weinstein
Department of Physics, Old Dominion University, Norfolk, Virginia 23529

Glen A. Warren
Department of Physics, Laboratory for Nuclear Science and Bates Accelerator Center, Massachusetts Institute of Technology, Cambridge, Massachusetts 02139
(Received 10 January 1994)

Unexplained anomalies in quasielastic (e, e') measurements motivated $(e, e'p)$ experiments to determine the reaction mechanisms (single-nucleon knockout, multinucleon knockout, delta production, etc.) involved in quasielastic electron scattering. In this paper we use various models to extrapolate from C$(e, e'p)$ measurements, where an outgoing proton is detected in a small solid angle centered around the virtual photon angle, to C(e, e') measurements, which integrate over all knockedout particles at all angles. Extrapolated single nucleon knockout (p and s shell) only accounts for 25% of the (e, e') cross section in the dip region and only 40 – 60% in the quasielastic region. This indicates that the "quasielastic" region has a large nonquasielastic component. Various multinucleon knockout models (two-nucleon correlations, six-quark bags, and qualitative final state rescattering) are compared to C$(e, e'p)$ missing energy spectra and to the difference between the (e, e') cross section and the extrapolated single-nucleon knockout; none completely describe the data.

PACS number(s): 25.30.Fj, 21.10.Jx, 21.60.−n

I. INTRODUCTION

Interactions with uncorrelated single nucleons were expected to dominate the nuclear electromagnetic response at quasielastic kinematics, $\omega = q_\mu^2/2m_p$ (q_μ and ω are the four-momentum and energy transfers). However, quasielastic electron scattering (e, e') measurements cannot be explained solely in terms of interactions with single-nucleon currents. The unexplained anomalies include the change in the ratio of the reduced response functions f_T/f_L between $A = 3$ and $A \geq 4$ [1,2], the deficiency of the Coulomb sum [3,4], and more generally, the inability of theory to explain both the longitudinal and the transverse response functions [5,6]. These anomalies motivated the performance of a number of C$(e, e'p)$ experiments to elucidate the reaction mechanisms and currents involved in quasielastic electron scattering [7–10]. These experiments had two major results: (1) The cross section for single-nucleon $(e, e'p)$ knockout was only 50–60 % of that predicted by distorted wave impulse approximation (DWIA) analysis (assuming 100% shell-model occupation) in general agreement with results from other $(e, e'p)$ experiments [11] and (2) a large fraction of the cross section is at large missing energies (large excitation energy of the residual nuclear system) and is attributed to multinucleon knockout. In this paper, we will attempt to connect the results of these $(e, e'p)$ experiments to (e, e') measurements conducted at the same electron kinematics in order to estimate what fraction of the inclusive (e, e') cross section stems from single-nucleon interactions and what fraction stems from two- or more-nucleon interactions. Since this connection between $(e, e'p)$ and (e, e') is model dependent, we will simultaneously test various models of quasielastic scattering.

II. DATA

We will compare C(e, e') data to C$(e, e'p)$ data at several sets of energy and momentum transfer:

$$\begin{aligned}(q, \omega) = (400, 120) &\quad \text{quasielastic,}\\ (400, 200) &\quad \text{dip,}\\ (585, 210) &\quad \text{quasielastic,}\\ (775, 355) &\quad \text{quasielastic.}\end{aligned} \tag{1}$$

The $q = 400$ MeV/c quasielastic measurement was performed at two angles in order to separate the longitudinal and transverse response functions. The C$(e, e'p)$ experiments were performed at the Bates Linear Accelerator Center using standard magnetic spectrometers ($\Delta\Omega_e \approx 10-20$ msr, $\Delta\Omega_p = 3.8$ msr). The electron spectrometer was configured to select $\mathbf{q}$ and ω. The proton was detected along the direction of the momentum transfer, $\mathbf{p}_f \parallel \mathbf{q}$. Only protons emerging in a cone of size $\Delta\Omega_p$ around $\mathbf{q}$ were detected. The cross section was measured as a function of missing energy, $\epsilon_m = \omega - T_p$, where T_p is the kinetic energy of the detected proton. The C$(e, e'p)$ data have three prominent features (see Fig. 1): a narrow peak centered at $\epsilon_m \approx 18$ MeV corresponding to p-shell proton knockout, a wide peak centered at $\epsilon_m \approx 35$ MeV corresponding to s-shell proton knockout, and a long flat tail extending out to very large missing energies corresponding to multinucleon knockout.

The C(e, e') data come from several sources. The data at $q = 400$ MeV/c and $q = 585$ MeV/c come from C(e, e') measurements at Saclay [3] and from inclusive data measured simultaneously with the C$(e, e'p)$ data [12]. The two data sets agree. The C(e, e') data at $q = 775$ MeV/c

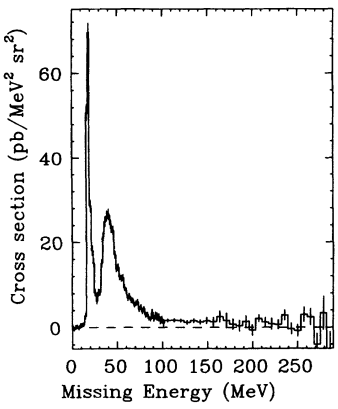

FIG. 1. Cross section versus missing energy for C$(e,e'p)$ at $q = 775$ MeV/c and $\omega = 355$ MeV.

come only from the inclusive data measured simultaneously with the C$(e,e'p)$ data.

III. PROCEDURE

In order to extrapolate from these limited proton-solid-angle C$(e,e'p)$ measurements to inclusive (e,e') processes which include all ejected particles at all angles, we need to calculate an extrapolation factor. To do this, we use a model to calculate the cross section for $(e,e'p)$ where the proton was ejected in the solid angle of the spectrometer, $\sigma^{\rm calc}_{\rm detected}$, and also the cross section for $(e,e'p)$ and $(e,e'n)$ where the nucleon was ejected in any direction, $\sigma^{\rm calc}_{\rm total}$. The extrapolated cross section is then the observed C(e,$e'p$) cross section divided by the calculated detected $(e,e'p)$ cross section times the calculated total cross section:

$$\frac{d\sigma^i_{\rm extrap}}{d\Omega_e d\omega} = \frac{d\sigma^i_{\rm observed}}{d\Omega_e d\Omega_p d\omega}\left(\frac{\frac{d\sigma^{\rm calc}_{\rm total}}{d\Omega_e d\omega}}{\frac{d\sigma^{\rm calc}_{\rm detected}}{d\Omega_e d\Omega_p d\omega}}\right)^i, \tag{2}$$

where i refers to the reaction process (p-shell, s-shell, or multinucleon knockout) and $d\sigma^i_{\rm observed}/d\Omega_e d\Omega_p d\omega$ is integrated over the appropriate missing energy for process i. The total extrapolated inclusive (e,e') cross section is then

$$\frac{d\sigma_{\rm extrap}}{d\Omega_e d\omega} = \frac{d\sigma^p_{\rm extrap}}{d\Omega_e d\omega} + \frac{d\sigma^s_{\rm extrap}}{d\Omega_e d\omega} + \frac{d\sigma^{\text{multi-}N}_{\rm extrap}}{d\Omega_e d\omega}. \tag{3}$$

This technique is sensitive only to the angular distributions predicted by the various models and not to the overall normalization of each model.

Summing the reaction processes independently to obtain the total extrapolated inclusive (e,e') cross section is a valid approach if each process can be cleanly distinguished in the missing energy spectrum. The p shell is distinct, but there is no clear boundary between the s-shell and multinucleon contributions.[1] Since, at $q = 400$ MeV/c, the longitudinal response function R_L is consistent with zero for $\epsilon_m \geq 50$ MeV [8], we infer that single-nucleon knockout does not contribute to the cross section for $\epsilon_m \geq 50$ MeV. Since in both Li$(e,e'p)$ and C$(e,e'p)$, the transverse/longitudinal ratio increases at the two-nucleon knockout threshold [13,14], we infer that multinucleon processes begin at that threshold, which is 28 MeV for ^{12}C.

For purposes of this calculation, we will consider $\epsilon_m = 50$ MeV as a boundary below which only single-particle emission contributes to the cross section and above which only multinucleon emission contributes. As a result of this simplification, we overestimate the single-nucleon contribution to the inclusive cross section and underestimate the multinucleon contribution. Despite this underestimate, this paper will show that multinucleon knockout is very large even at quasielastic kinematics.

There are two useful approximations for calculating and thinking about the $(e,e'N)$ process. In the plane wave impulse approximation (PWIA) the virtual photon is absorbed on a single nucleon, that nucleon is detected, and that nucleon does not interact with the residual nucleus. In this simple case the recoil momentum $\mathbf{p}_{\rm recoil} = \mathbf{q} - \mathbf{p}_N$, where p_N is the momentum of the detected struck nucleon, is equal to the negative of the struck nucleon's initial momentum in the nucleus. The missing energy $\epsilon_m = \omega - T_N$, where T_N is the kinetic energy of the detected nucleon, is the excitation energy of the residual nuclear system plus the binding energy of the valence nucleon (16 MeV for a p-shell proton in ^{12}C).[2] In the PWIA, the $(e,e'N)$ cross section factorizes

$$\frac{d^6\sigma}{d\Omega_e d\Omega_N d\omega d\epsilon_m} = K\sigma_{eN} S(\epsilon_m, p_{\rm recoil}), \tag{4}$$

where K is a kinematic factor. σ_{eN} describes the probability for scattering an electron from a nucleon where the nucleon is bound in the initial state and unbound in the final state. This "half-off-shell" cross section cannot be theoretically unambiguously calculated. We use the $cc1$ prescription for σ_{eN} given by de Forest [15]. $S(\epsilon_m, p_{\rm recoil})$ is the spectral function, the joint probability of finding a nucleon in the nucleus, the knockout of which would leave the residual nucleus with missing energy ϵ_m and recoil momentum $p_{\rm recoil}$.

In the distorted wave impulse approximation (DWIA), the outgoing struck nucleon does interact with the residual nucleus. In this case, the energy and momentum of the outgoing nucleon will be distorted by its interaction with the residual nucleus and the simple PWIA picture will be slightly altered. The cross section still factorizes in some cases. We will include the effects of final state interactions in a simplified way that does not destroy the simple PWIA picture. The DWIA will be discussed in greater detail later.

The extrapolation from $(e,e'p)$ to (e,e') is a large one. The area bounded by the solid lines in Fig. 2 shows

[1] This is especially true because a carbon nucleus with an s-shell hole will deexcite via nucleon emission in about the same time it takes the outgoing struck nucleon to exit the nucleus.

[2] Note that this definition assumes that T_{A-1}, the kinetic energy of the residual nucleus, is small; this is reasonable for ^{12}C and not reasonable for deuterium.

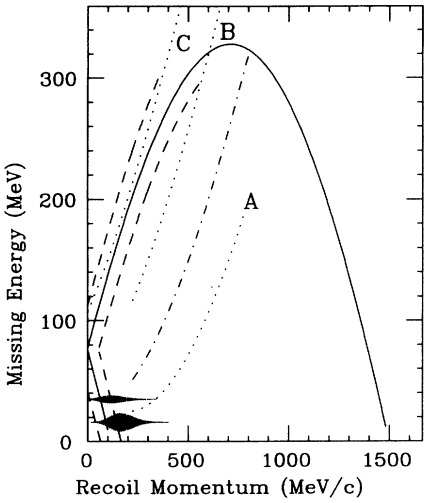

FIG. 2. Kinematic limits and spectral functions for $q = 775$ MeV/c and $\omega = 355$ MeV. The solid line indicates the kinematic limits for (e,e'). The area bounded by the dashed lines indicates the kinematics sampled by the parallel kinematics C$(e,e'p)$ experiment. The parallel vertical lines at $\epsilon_m = 18$ and 35 MeV show $p_r^2 \cdot n_p(p_r)$ and $p_r^2 \cdot n_s(p_r)$, the p- and s-shell momentum distributions, respectively. The dotted and dash-dotted lines refer to a simple two-nucleon correlation knockout mechanism described in the text. The dash-dotted line indicates the centroid of the $2N$ missing energy distribution, the dotted lines labeled A and B show the limits of the missing energy distribution for $p_{\text{c.m.}} \leq 200$ MeV/c and the dotted line labelled C shows the upper limit of the missing energy distribution for $p_{\text{c.m.}} \leq 400$ MeV/c. All of those curves are for no excitation of the residual nucleus ($E^{2N}_{\text{thresh}} = 25$ MeV). Note that the uppermost dotted line is within the kinematic acceptance of the C$(e,e'p)$ measurement, indicating that correlated two-nucleon knockout could contribute to the cross section at large missing energies. Multinucleon knockout mechanisms, if any, will populate the large missing energy ($\epsilon_m > 50$ MeV) region.

the range of recoil momentum and missing energy accessible to an $(e,e'N)$ experiment for momentum transfer, $q = 775$ MeV/c, and energy transfer, $\omega = 355$ MeV (assuming we could place our nucleon detector anywhere and detect nucleons of any desired energy). If we think of the (e,e') reaction as the integral over available phase space of the $(e,e'N)$ reaction [where $(e,e'N)$ includes both $(e,e'p)$ and $(e,e'n)$], then the area bounded by the solid lines shows the phase space available to the (e,e') reaction. In the PWIA, $p_{\text{recoil}} = p_{\text{initial}}$ and $\epsilon_m = \epsilon_{\text{excit}} + \epsilon_b$, where ϵ_b is the binding energy of the valence nucleon. Thus the solid lines indicate the phase space available to the (e,e') reaction in initial-momentum–excitation-energy space. The dashed lines indicate the limits of p_{recoil} and ϵ_m sampled by the C$(e,e'p)$ measurement of Ref. [9].[3] This picture overstates the relative phase space available to the $(e,e'p)$ reactions because the real phase space is four dimensional $(\epsilon_m, \mathbf{p}_{\text{recoil}})$ rather than two dimensional $(\epsilon_m, p_{\text{recoil}})$. The $(e,e'p)$ measurements are in parallel kinematics and thus sample only a limited angular range in θ_{recoil}. Thus the (e,e') reaction, in addition to including both proton and neutron knockout, also includes a much larger range of ϵ_m and $\mathbf{p}_{\text{recoil}}$ than the $(e,e'p)$ reaction.

To calculate the extrapolation factor between $(e,e'p)$ and (e,e'), we need to weigh the available phase space with the spectral function. In the absence of final state interactions (i.e., in the PWIA), the spectral function $S(\epsilon_m, p_{\text{recoil}})$ is the joint probability of finding a nucleon in the nucleus with binding energy ϵ_m and initial momentum p_{recoil}. The vertical bars centered at $\epsilon_m = 18$ MeV and $\epsilon_m = 35$ MeV indicate the single-nucleon knockout p- and s-shell momentum distributions. The size of the bar indicates $p^2 \cdot n(p)$, the recoil momentum squared times the relative magnitude of the harmonic oscillator momentum distribution at that recoil momentum. Note that, as expected, the s-shell momentum distribution peaks at around 100 MeV/c and the p-shell momentum distribution peaks at around 160 MeV/c. We neglect the smaller excited states (e.g., $1p_{\frac{1}{2}}$). This is at most a 10% effect. The plot does not show the range of the s shell in missing energy (25 – 50 MeV). The $(e,e'p)$ measurement sampled a reasonable range of the single-nucleon knockout phase space. The graph overstates the amount sampled because it does not show the experimental acceptances in three dimensions (in $\mathbf{p}_{\text{recoil}}$ space), only in one dimension (in $|\mathbf{p}_{\text{recoil}}|$ space).

One example of a multinucleon knockout mechanism is the knockout of a correlated two-nucleon pair. Here we assume that the pair is highly correlated and can have very large relative momentum (p_{rel}) but has relatively small momentum with respect to the $A-2$ system ($p_{\text{c.m.}}$). We assume that the virtual photon is absorbed on one nucleon and that the second (undetected) nucleon leaves the nucleus. In this very simple model the missing momentum for this reaction is

$$p_{\text{recoil}} = \mathbf{q} - \mathbf{p_N} = -\mathbf{p_{rel}} - \frac{1}{2}p_{\text{c.m.}} \quad . \tag{5}$$

The missing energy is

$$\epsilon_m = E^{2N}_{\text{thresh}} + \sqrt{\left(-\mathbf{p_{rel}} + \frac{1}{2}\mathbf{p}_{\text{c.m.}}\right)^2 + m^2} - m \ , \tag{6}$$

ignoring the excitation energy and the recoil kinetic energy of the $A-2$ system. Including various excitations of the $A-2$ system will spread the strength to larger missing energies. The dash-dotted line in Fig. 2 shows the centroid of the missing energy distribution, the dotted lines labeled A and B show the limits of the missing energy distribution for $p_{\text{c.m.}} \leq 200$ MeV/c, and the dotted line labeled C shows the upper limit of the missing energy distribution for $p_{\text{c.m.}} \leq 400$ MeV/c. All of those curves are for no excitation of the residual nucleus ($E^{2N}_{\text{thresh}} = 25$ MeV). Note that the uppermost dotted line is within the kinematic acceptance of the C$(e,e'p)$ measurement, indicating that correlated two-nucleon knockout could con-

[3]The C$(e,e'p)$ kinematic limits exceed the (e,e') limits because of finite experimental acceptances (that is, $\Delta q, \Delta\omega, \ldots \neq 0$).

tribute to the cross section at large missing energies.

This figure indicates the degree of extrapolation required at (q = 775 MeV/c, ω = 355 MeV) to compare the C$(e,e'p)$ and C(e,e') cross sections. We must extrapolate the single-nucleon knockout spectral functions from the sampled range of 25 < $p_{\rm recoil}$ < 150 MeV/c at parallel kinematics to the entire accessible range of 25 - 1500 MeV/c. We must extrapolate the multinucleon knockout cross section from the narrow range sampled [approximately along the line from ($p_{\rm recoil}, \epsilon_m$) = (0,80) - (500,300)] to the entire parabola bounded by the solid lines.

IV. MODELS

We will need models to perform these extrapolations. In all of the models we will consider, the electron interacts with a single nucleon which is either uncorrelated (single-nucleon knockout) or correlated with other nucleons either via initial state or final state correlations.

A. Single-nucleon knockout models

We consider two shell-model spectral functions for the single-nucleon contributions: harmonic oscillator (HO) and Woods-Saxon (WS). The spectral function for the shell-model state α with binding energy ϵ_α and momentum distribution $n_\alpha(p_i)$ is

$$S_\alpha(p_i,\epsilon_m) = n_\alpha(p_i)\delta(\epsilon_m - \epsilon_\alpha). \tag{7}$$

For example, the spectral function in the HO model for ^{12}C is

$$S_S(p_i,\epsilon_m) = \left(\frac{b}{\sqrt{\pi}}\right)^3 \exp\left[-(p_i b)^2\right]\delta(\epsilon_m - \epsilon_S), \tag{8}$$

$$S_P(p_i,\epsilon_m) = \frac{2}{3}(p_i b)^2\left(\frac{b}{\sqrt{\pi}}\right)^3 \exp\left[-(p_i b)^2\right]\delta(\epsilon_m - \epsilon_P), \tag{9}$$

$\hbar$ = 1, c = 1. We used a HO constant b = 1.7 fm. We generated the Woods-Saxon momentum distributions from $\phi(r)$, a coordinate space wave function calculated using the Elton-Swift proton potential [16]. We used binding energies of 34 MeV and 16 MeV for the S and P shells, respectively.

We calculated both single-neutron and single-proton knockout. We found that quasielastic neutron knockout was about 10 - 40% as large as quasielastic proton knockout (depending on kinematics). We include neutron knockout in the final single-nucleon knockout results.

For the single-nucleon emission calculations, we considered the effects of final state interactions (FSI's) using an optical potential. The real part of the optical potential shifts the average final proton momentum:

$$\mathbf{p}_f \approx \left(1 - \frac{E_f V_{\rm eff}}{p_f^2}\right)\mathbf{p}'_f, \tag{10}$$

where $V_{\rm eff}$ is the average over the interaction region of the real part of the optical potential, $\mathbf{p}'_f$ is the momentum of the nucleon immediately after scattering ($\mathbf{p}_i = \mathbf{p}'_f - \mathbf{q}$), and $\mathbf{p}_f$ is the measured asymptotic momentum of the nucleon. We determined the average value of $V_{\rm eff}$ by inspection of various optical potentials [17–19]. The average values of the real parts of the optical potential are given in Table I. This crude determination is acceptable for two reasons: First, the extrapolation is not very sensitive to $V_{\rm eff}$, and second, $V_{\rm eff}$ is optical model dependent and hence not well determined. We consider a range of ±5 MeV in $V_{\rm eff}$ to estimate the uncertainty of this effect. These uncertainties are approximately 3%.

TABLE I. Effective real part of the optical potential (MeV).

(q,ω)	(400, 200)	(400, 120)	(585, 210)	(775, 355)
S shell	-10	-25	-10	15
P shell	-10	-20	-5	15

Final state interactions also cause protons to scatter out of the elastic channel. Thus, in an $(e,e'p)$ experiment, protons which would, in the absence of final state interactions, be detected in the proton spectrometer are rescattered by the residual nucleus and are not detected. This decreases the $(e,e'p)$ cross section. We need to correct for this effect in order to compare the $(e,e'p)$ and (e,e') cross sections.[4]

The effect of these final state interactions is usually described by the imaginary part of the optical potential which models the loss of flux from the elastic channel into other channels. Proton-nucleus optical potentials are determined by a best fit to elastic proton scattering data. Unfortunately, $(e,e'p)$ proton-nucleus interactions are very sensitive to the details of the proton wave function in the nucleus, which are not well constrained by elastic scattering data. DWIA calculations using different optical models predict $(e,e'p)$ cross sections that vary by around 10%.

We estimate the effects of the final state interactions by comparing $(e,e'p)$ single-nucleon knockout cross sections calculated with and without an optical potential. The calculated plane wave impulse approximation (no-FSI) cross section was ≈ 30% larger than the calculated distorted wave impulse approximation (FSI) cross section for these C$(e,e'p)$ experiments. The uncertainty of the amount of this reduction is approximately 10%. We will use this factor of 1.3 ± 0.1 to correct the extrapolated $(e,e'p)$ cross sections for the effects of final state interactions.

B. Multinucleon knockout models

We investigated three models of multinucleon knockout: an initial state two-nucleon ($2N$) correlation spec-

[4] In parallel kinematics, protons rescattering into the spectrometer are at most 5% of the continuum cross section [12] and can be neglected here. This is not necessarily true in nonparallel kinematics.

tral function [20, 21], a simple six-quark bag model [22], and a two-nucleon and three-nucleon phase space calculation based on a zero-range final state interaction [23]. Note that in all of these models the electron interacts with a single nucleon; these models incorporate multinucleon correlations, not multinucleon currents. The interaction of the virtual photon with an exchanged meson is not included in these models; this would be one type of multinucleon current.

To explain the strength at high missing momentum and high missing energy, Ciofi degli Atti *et al.* [20] developed a method to calculate the $2N$-correlation spectral function for all nuclei. They determined the $2N$-correlation spectral function for ^{3}He and for nuclear matter from first principles. The calculation assumes that the two correlated nucleons are close together and that the rest of the nucleus is far away from this $2N$ pair. For this reason, this model is valid only for high recoil momentum and high missing energy states. Interpolating between $A = 3$ and $A = \infty$, they obtained the ^{12}C $2N$-correlation spectral function. The spectral function is calculated with the realistic momentum distributions determined from variational calculations on ^{12}C. An example of the resulting missing energy spectrum is shown in Fig. 3.

The six-quark bag model of Mulders [22] assumes that the electron scatters from a $2N$ system exciting it to some six-quark excited state. This six-quark system then decays isotropically in its center-of-mass frame back into two nucleons. We assume that the residual nucleus does not recoil. The initial momentum distribution of the six-quark system is determined by convoluting the HO momentum distributions for different shells:

$$N_{\alpha\beta}(p) = \int d^3\mathbf{p}_1 d^3\mathbf{p}_2 N_\alpha(p_1) N_\beta(p_2) \delta^3(\mathbf{p}_1 + \mathbf{p}_2 - \mathbf{p}). \tag{11}$$

We normalized the momentum distributions to $\int N(p) 4\pi p^2 dp = 1$. For purposes of calculating the unnormalized momentum distribution by summing over all pairs of nucleons we assumed a 5:2 p-shell to s-shell ratio (consistent with measured spectroscopic factors). This gives 20 p-shell–p-shell (PP) pairs, 10 p-shell–s-shell (PS) pairs, and 1 s-shell–s-shell (SS) pair for a proton-proton system. For a neutron-proton system, there are 25 PP, 20 PS, and 4 SS pairs. The final extrapolated cross section is relatively insensitive to the choice of pair weightings and we used those from pp pairs. Overall normalization of the $2N$ systems drops out because of the use of ratios of the cross sections. We used pair binding energies of 30 MeV, 45 MeV, and 60 MeV for PP, PS, and SS pairs, respectively. An example of the resulting missing energy spectrum is given in Fig. 4.

The zero-range interaction model of Takaki predicts the available $2N$ and $3N$ phase space using qualitative final state interactions [23]. For the $2N$ cross section, an electron scatters off of one nucleon, which propagates and then interacts with another nucleon via a delta function potential. This model assumes that the center of mass of the nucleus is fixed and that the bound nucleons are described by s-shell HO wave functions. Only longitudinal coupling between the nucleon and electron is considered. Since a quantitative calculation using this model underestimates the dip region continuum strength by a factor of 10, we use this model only to predict the available $2N$ and $3N$ phase space. The $2N$ cross section is given by

$$d\sigma \propto p p_f \exp\left[-[(\mathbf{p}_f - \mathbf{q})^2 + \mathbf{p}^2]\frac{b^2}{2}\right] j_0\big(ipb^2|\mathbf{p}_f - \mathbf{q}|\big), \tag{12}$$

where $\mathbf{p}$ and $\mathbf{p}_f$ are the final momentum of the undetected and detected nucleon respectively, b is the HO constant, and j_0 is the spherical Bessel function.

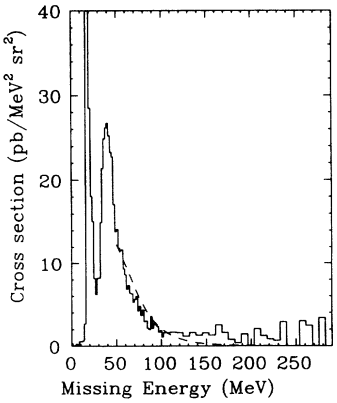

FIG. 3. C$(e, e'p)$ cross section versus missing energy for the $2N$ correlation model for $q = 775$ MeV/c and $\omega = 355$ MeV (dashed line) compared to the data (solid histogram). The vertical scale has been truncated to better display the model. The model has been scaled by an arbitrary factor.

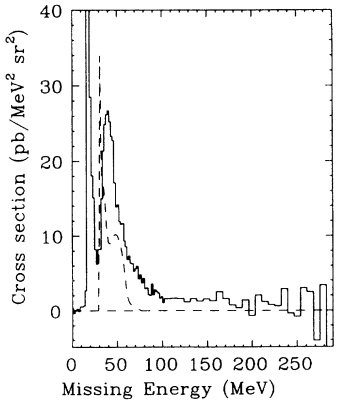

FIG. 4. C$(e, e'p)$ cross section versus missing energy for the six-quark bag model of Mulders for $q = 775$ MeV/c and $\omega = 355$ MeV (dashed line) compared to the data (solid histogram). The vertical scale has been truncated to better display the model. To account for the broad s-shell peak, the PS pair distribution was convoluted with a parabola 30 MeV wide. Likewise, the SS pair distribution was convoluted twice with the parabola.

If the center of mass of the two interacting nucleons is fixed, then conservation of energy and momentum uniquely relates the angle of the scattered nucleons, the missing energy, and the binding energy of the pair:

$$\cos\left(\theta_{pq}^{2N}\right) = \frac{q^2 + (\omega + m - \epsilon_m)^2 - (\epsilon_m - \epsilon_b + m)^2}{2q\sqrt{(\omega + m - \epsilon_m)^2 - m^2}}. \tag{13}$$

θ_{pq}^{2N} is the angle of the detected proton with respect to $\mathbf{q}$.

To allow for the broad s shell, we integrated over a range of missing energies. The lower limit of the missing energy was determined by the curve for $\epsilon_b = 30$ MeV, but the curve is shifted in ϵ_m so that at $\theta_{pq} = 0$ the curve passes through $\epsilon_m = 30$ MeV. The upper limit was determined by the $\epsilon_b = 60$ MeV curve shifted by 15 MeV in missing energy.

For the $3N$ cross section of Takaki, the scattered nucleon interacts with two other nucleons via a delta function potential. The assumptions of $2N$ scattering also apply to $3N$ scattering. The $3N$ cross section is

$$d\sigma \propto \int_0^{p'_{\max}} dp'\, p\, p_f\, p'^2 \exp\left[-[(\mathbf{p}_f - \mathbf{q})^2 + k'^2]\frac{b^2}{3}\right] j_0\left(i\frac{2}{3}pb^2|\mathbf{p}_f - \mathbf{q}|\right), \tag{14}$$

$$p'_{\max} = \sqrt{4m(\omega - 3\epsilon_h - T_{k_f})}, \tag{15}$$

where $\mathbf{p}$ and $\mathbf{p}'$ are the relative and center-of-mass momentum for the undetected particles respectively and $\epsilon_h = 15$ MeV is the energy to remove a single nucleon from the nucleus. For fixed center of mass of the three interacting nucleons, conservation of energy and momentum restrict the range of θ_{pq}^{3N} of the detected nucleon:

$$\cos\theta_{pq}^{3N} \leq \frac{q^2 + 3m^2 + (\omega + m - \epsilon_m)^2 - (\epsilon_m - \epsilon_b + 2m)^2}{2q\sqrt{(\omega + m - \epsilon_m)^2 - m^2}}. \tag{16}$$

Figure 5 shows the values of θ_{pq} for $2N$ and $3N$ final state interactions that contribute to the coincidence cross section plotted versus missing energy for one set of kinematics.

While the delta function interaction simplifies the evaluation of the cross sections, it leaves the cross sections unnormalized. We determine the relative weighting of the $2N$ and $3N$ reaction mechanisms by analytically fitting them to the measured missing energy cross section for $\epsilon_m \geq 50$ MeV. Although we fit the $2N$ and $3N$ curves to the data for $\epsilon_m > 50$ MeV, the $2N$ cross section is large for $\epsilon_m < 50$ MeV. An example of this curve fit is shown in Fig. 6.

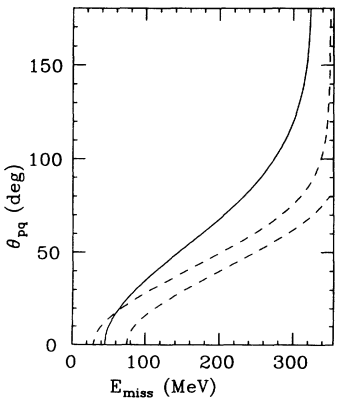

FIG. 5. Restrictions on θ_{pq} versus missing energy for $q = 775$ MeV/c and $\omega = 355$ MeV. The dashed lines are the kinematic limits for two-nucleon knockout. The solid line is the maximum allowed θ_{pq} for three-nucleon knockout.

The $3N$ interaction has a larger angular distribution than the $2N$ interaction. By fitting the relative weights of the $2N$ and $3N$ interactions, we determine an average angular distribution for all multinucleon processes (within this model). If there is more $3N$, then the angular distribution is broader; if there is more $2N$, then the angular distribution is narrower. To estimate the uncertainty of this calculation, we consider different relative weightings of the $2N$ and $3N$ reaction mechanisms. We calculated the effective solid angles for 0.5 and 1.5 times the analytically determined $2N$:$3N$ weighting ratio. We set the

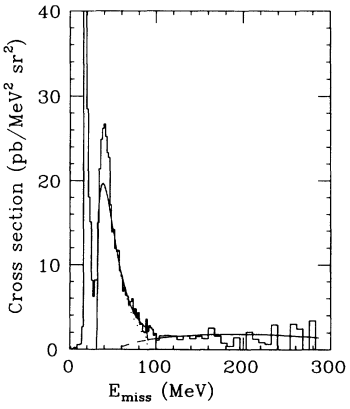

FIG. 6. Example of analytical fit of $2N$ and $3N$ parts of Takaki's delta function interaction for $q = 775$ MeV/c and $\omega = 355$ MeV. The dotted line is the $2N$ contribution, the dashed line is the $3N$ contribution, and the solid curve is the sum of the $2N$ and $3N$ contributions. The histogram is the C$(e,e'p)$ data.

TABLE II. Measured $(e, e'p)$ cross sections (pb/MeV sr^2) integrated over the different reaction mechanisms. QE refers to quasielastic kinematics.

(q, ω)	(400, 200) Dip	$(400,120)_{\text{fwd}}$ QE	$(400,120)_{\text{bck}}$ QE	(585, 210) QE	(775, 355) QE
S shell	474 ± 35	5040 ± 140	1230 ± 30	998 ± 10	430 ± 6
P shell	1730 ± 35	4590 ± 130	896 ± 24	722 ± 9	348 ± 7
Continuum	3675 ± 119			567 ± 33	463 ± 25

uncertainty large enough to include these two extreme cases. These uncertainties are approximately 10%.

V. RESULTS AND CONCLUSIONS

The results of the various measurements and calculations are shown in Tables II–IV. Table II shows the measured $(e, e'p)$ cross sections for each reaction mechanism integrated over the appropriate range of missing energy. Table III shows the calculated extrapolation factors (as defined in Sec. III). These factors include the factor of 1.3 ± 0.1 to account for final state interactions. The cross section for $(e, e'n)$ has been included in the single-nucleon knockout extrapolation factor. The $(e, e'n)$ cross section has not been included in the multinucleon knockout models. The extrapolation factors are shown separately for each process and each model. Thus we are extrapolating the single-nucleon knockout cross section by a factor of 36–230 and we are extrapolating the multinucleon knockout cross section by a factor of 100 – 1500. We multiplied the measured $(e, e'p)$ cross sections by 3.8 msr (the proton solid angle) and by the appropriate extrapolation factor to get the extrapolated cross section. Table IV shows the extrapolated cross sections and the measured (e, e') cross sections. The "Single nucleon" entries are the average of the HO and WS single-nucleon knockout extrapolated cross sections. The "Extrap/measured" row contains the ratio of the FSI-corrected $C(e, e'p)$ extrapolations divided by the measured $C(e, e')$ cross sections.

There are several interesting points to note in the comparison of the extrapolated single-nucleon $(e, e'p)$ cross section to the measured (e, e') cross section.

(1) The extrapolated single-nucleon $(e, e'p)$ cross section, when corrected for the effects of final state interactions, accounts for only 25 – 60 % of the (e, e') cross section (25% in the dip region and 40 – 60 % in the quasielastic region). Figure 7 shows a comparison of the (e, e') and $(e, e'p)$ cross sections at $q = 585$ MeV/c.

(2) The extrapolated single-nucleon $(e, e'p)$ cross section is insensitive to the single-nucleon momentum distribution used. The harmonic oscillator and Woods-Saxon models yield similar results.

(3) The extrapolated single-nucleon $(e, e'p)$ cross section accounts for a much lower fraction of the inclusive (e, e') strength in the dip region ($q = 400$ MeV/c, $\omega = 200$ MeV) than in the quasielastic region. This ratio of 0.26 ± 0.03 is consistent with the proportion of (e, e') dip region strength accounted for by single-nucleon knockout calculations [24].

(4) At $q = 400$ MeV/c and $\omega = 120$ MeV we see a small difference between the forward angle measurement, where the virtual photon polarization $\epsilon = 0.576$, and the backward angle measurement, where $\epsilon = 0.131$. At the forward angle, the extrapolated single-nucleon knockout $(e, e'p)$ cross section is 58% of the measured (e, e') cross section; at the backward angle it is 51%. This difference is consistent with an additional non-single-nucleon transverse reaction mechanism. This reaction mechanism would enhance the inclusive transverse response but leave the single-nucleon knockout unchanged.

There is much more variation in the multinucleon

TABLE III. Extrapolation factors for $C(e, e'p) \rightarrow C(e, e')$. Multiply the measured $(e, e'p)$ cross sections by 3.8 msr (the proton solid angle) and by the appropriate extrapolation factor to get the extrapolated cross section. These extrapolation factors include the effect of absorption in the final state interaction (a factor of 1.3). "2NC" refers to the two-nucleon correlation theory of Ref. [20], "Takaki" refers to the qualitative final state rescattering model of Ref. [23], and "six quark" refers to the six-quark model of Ref. [22].

(q, ω)	(400, 200) Dip	$(400,120)_{\text{fwd}}$ QE	$(400,120)_{\text{bck}}$ QE	(585, 210) QE	(775, 355) QE
	Single nucleon				
HO: S	79 ± 9	101 ± 12	108 ± 12	57 ± 7	36 ± 4
HO: P	96 ± 10	223 ± 23	231 ± 25	216 ± 23	109 ± 12
WS: S	88 ± 10	108 ± 12	114 ± 13	61 ± 7	38 ± 4
WS: P	112 ± 12	215 ± 26	218 ± 26	192 ± 21	101 ± 12
	Multinucleon				
2NC	184			200	230
Takaki	760			550	500
Six quark	1300	400	400	740	790

TABLE IV. Measured and extrapolated inclusive cross sections (pb/MeV sr).

(q,ω)	(400, 200) Dip	$(400,120)_{fwd}$ QE	$(400,120)_{bck}$ QE	(585, 210) QE	(775, 355) QE
Measured	3200 ± 140	10000 ± 300	2560 ± 70	1279 ± 174	466 ± 69
Extrapolated	Single nucleon				
	840 ± 110	5810 ± 800	1300 ± 170	780 ± 100	200 ± 26
Extrap/measured	0.26 ± 0.04	0.58 ± 0.10	0.51 ± 0.08	0.61 ± 0.16	0.43 ± 0.12
Extrapolated	Multinucleon				
2NC	6300			430	400
Takaki	10600			1210	870
Six quark	18200			1570	1370

knockout models. Since the single-nucleon knockout models are more believable, we compare the multinucleon knockout models to the (e,e') cross section minus the extrapolated single-nucleon knockout cross section. We do this for all data sets except the $q = 400$ MeV/c quasielastic data which did not measure a large enough range of missing energy for comparisons.

(1) The missing energy distribution predicted by Mulders' model [22] does not provide enough cross section at large missing energy, $\epsilon_m > 80$ MeV (see Fig. 4). In addition, this cross section is a factor of 2 – 6 larger than the inclusive cross section minus the extrapolated single-nucleon knockout cross section.

(2) The missing energy distribution predicted by Takaki's model [23] matches the observed $(e,e'p)$ continuum data ($\epsilon_m > 50$ MeV) well (with only two fit parameters). However, the fit two-nucleon knockout cross section also accounts for almost all of the observed s-shell ($25 < \epsilon_m < 50$ MeV) cross section. This leads us to question the calculation. The shape of the two-nucleon knockout cross section is also different from the measured shape of $S_T - S_L$ [8]. The cross section is a factor of 2 – 4 larger than the inclusive cross section minus the extrapolated single-nucleon knockout cross section.

(3) The two-nucleon correlation model of Simula [21] and Ciofi degli Atti [20] matches the $q = 775$ MeV/c $(e,e'p)$ data nicely (with an arbitrary scale factor) from $\epsilon_m = 50$ to 120 MeV but it does not provide enough cross section at larger missing energies. Otherwise, it has the closest agreement with the data. When compared to the inclusive cross section minus the extrapolated single-nucleon knockout cross section this model agrees at $q = 585$ and at $q = 775$ MeV/c and is a factor of 2 too large in the dip region.

The multinucleon knockout models encompass a range of ideas, from six-quark excited states to two-nucleon correlations to qualitative final state interactions. None of these models modify the current operator, and hence none of these models are true multinucleon models. Only the two-nucleon correlation model of Simula and Ciofi degli Atti comes close to both explaining the missing energy cross section distribution and accounting for the non-single-nucleon (e,e') yield for all of the data sets examined.

Only 40 – 60% of the quasielastic peak consists of quasifree nucleon knockout. The remainder of the cross section consists of some form of multinucleon knockout.

More detailed and less qualitative theories are needed to explain these data. Experimentally, soon experiments will be run using large acceptance spectrometers with continuous electron beam accelerators that will allow us to detect all of the knocked out hadrons in (e,e') measurements and directly test theories of multihadron knockout without resorting to crude extrapolations and approximations.

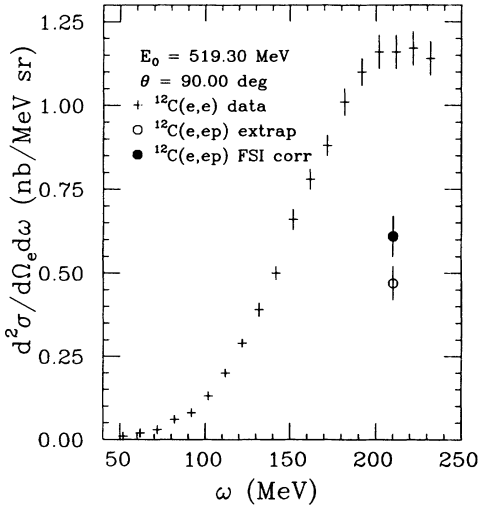

FIG. 7. Comparison of the extrapolated $C(e,e'p)$ cross section with the $C(e,e')$ cross section measured at Saclay at almost identical kinematics. The beam energy for the (e,e') measurement was 519 MeV; the beam energy for the $(e,e'p)$ measurement was 505 MeV. Both measurements were performed at $\theta_e = 90°$. The larger $C(e,e'p)$ point includes a factor of 1.3 to correct for the effects of final state interactions.

ACKNOWLEDGMENTS

The authors thank S. Simula and C. Ciofi degli Atti for supplying their two-nucleon correlation spectral function. The authors gratefully acknowledge the support of the Department of Energy (DE-AC02-76ER03069). L.B.W. gratefully acknowledges the support of Old Dominion University and the Continuous Electron Beam Accelerator Facility (CEBAF).

[1] A. Magnon (private communication).
[2] J.M. Finn, R.W. Lourie, and B.H. Cottman, Phys. Rev. C **29**, 2230 (1984).
[3] P. Barreau *et al.*, Nucl. Phys. **A402**, 515 (1983).
[4] Z.E. Mezziani *et al.*, Phys. Rev. Lett. **52**, 2130 (1984); **54**, 1233 (1985).
[5] G. Do Dang and N. Van Giai, Phys. Rev. C **30**, 731 (1984).
[6] L. Celenza *et al.*, Phys. Rev. C **31**, 212 (1985); L. Celenza *et al.*, *ibid.* **32**, 248 (1985); **32**, 650 (1985).
[7] R.W. Lourie *et al.*, Phys. Rev. Lett. **56**, 2364 (1986).
[8] P.E. Ulmer *et al.*, Phys. Rev. Lett. **61**, 2001 (1988).
[9] L.B. Weinstein *et al.*, Phys. Rev. Lett. **64**, 1646 (1990).
[10] G. van der Steenhoven *et al.*, Nucl. Phys. **A480**, 547 (1988).
[11] P.K.A. de Witt Huberts, J. Phys. G **16**, 507 (1990).
[12] R.W. Lourie, Ph.D. thesis, MIT, 1986; P.E. Ulmer, Ph.D. thesis, MIT, 1987; L.B. Weinstein, Ph.D. thesis, MIT, 1988.
[13] J.M.B. Lanen *et al.*, Phys. Rev. Lett. **64**, 2250 (1990).
[14] G. van der Steenhoven *et al.*, Nucl. Phys. **A484**, 445 (1988).
[15] T. de Forest, Jr., Nucl. Phys. **A392**, 232 (1983).
[16] L.B.B. Elton and A. Swift, Nucl. Phys. **A94**, 52 (1967).
[17] J. Comfort and B. Karp, Phys. Rev. C **21**, 2162 (1980).
[18] H.O. Meyer *et al.*, Phys. Rev. C **27**, 459 (1983).
[19] H.O. Meyer *et al.*, Phys. Rev. C **37**, 544 (1988).
[20] C. Ciofi degli Atti, S. Simula, L.L. Frankfurt, and M.I. Strikman, Phys. Rev. C **44**, R7 (1991).
[21] S. Simula (private communication).
[22] P.J. Mulders, Nucl. Phys. **A459**, 525 (1986).
[23] T. Takaki, Phys. Rev. Lett. **62**, 395 (1989).
[24] J.W. van Orden and T.W. Donnelly, Ann. Phys. (N.Y.) **131**, 451 (1981).